Chapter 1

Satellite Combined Radar-Radiometer algorithms

Mircea Grecu[1] and
William S. Olson[2]

Some abstract here.

1.1 Introduction

The benefit of incorporating radiometer observations into methodologies that estimate precipitation from space-borne radar observations was first realized by [1]. Specifically, due to size and weight limitations on antennae, space-borne radars operate at frequencies that make observations subject to attenuation. While attenuation correction methodologies exist, e.g. [2], variability in the size distribution of precipitation particles within the radar observing volume makes the attenuation correction process highly uncertain. At the same time, it had been recognized [3] that independent information regarding the Path-Integrated-Attenuation (PIA) may be used to reduce uncertainties in the attenuation correction process. PIA information independent of the radar measurements used in the attenuation correction process may be derived from the analysis of the electromagnetic power backscattered by the Earth's surface [3] and, as noted by Weinman et al. [1], low-frequency radiometer observations when available. The objective of the surface analysis is to estimate the power backscattered by Earth's surface in the absence of the rain. In the presence of rain, the ratio between the actual backscattered power and the estimated clear-sky backscattered power provides an estimate of the total attenuation from the radar to the Earth's surface [3] that can be used in attenuation correction and precipitation estimation process. The problem with the PIA estimation using this approach, usually referred to as the Surface Reference Technique (SRT), is that the estimation of the no-precipitation backscattered power may be highly uncertain in some situations. As recognized by Weinman et al. [1] and even earlier investigators, e.g. [4], radiometer observations over water surfaces at frequencies not associated with significant scattering (e.g. 10- and 19-GHz) contain information strongly related to the PIA. This

[1]GESTAR-II, Morgan State University and NASA GSFC
[2]GESTAR-II,UMBC and NASA GSFC

is because the emissivity of water surface is low and rain drops in the radiometer observing volume result in warmer brightness temperatures. The departure from the brightness temperature value expected in clear skies may be used to estimate the equivalent PIA at the radar operating frequency [1]. The initial study of Weinman et al. [1] provided a relationship between coincident radiometer observations at X-band and the associated PIA at X-band (9.6-GHz). Subsequent work Smith et al. [5] was carried out to determine a relationship between the PIA at Ku-band (13.8 GHz) and coincident radiometer observations 10.7-GHz. This relationship was developed for use in the Tropical Rainfall Measuring Mission (TRMM) [6] combined radar-radiometer algorithm [7].

However, although the relationships between low frequency brightness temperatures and the radar PIA at X- and Ku-band are well-defined and unambiguous, the use of satellite radiometer observations in satellite radar profiling algorithms is challenging. This because the typical footprints of low-frequency radiometer observations are significantly larger than the typical footprints of space-borne radars, which makes the radiometer observations difficult to translate into radar PIA. To overcome this difficulty various approaches akin to the downscaling of the radiometer observations to the radar footprint resolution have been developed [7, 8, 9, 10]. A common feature of these approaches was that the radar-footprint PIA was not directly estimated from the radiometer observations. Instead, optimization procedures were used to maximize the agreement between radiometer observations predicted from the radar observations and actual radiometer observations. While the impact of the radiometer observations on the final radar estimates is difficult to quantify, a clear benefit of combined radar-radiometer precipitation retrievals are consistent with both the radar and radiometer observations. Consequently, they may be used to derive large databases of precipitation and associated radiometer observations necessary in the development of "Bayesian" precipitation estimation algorithms from satellite radiometer-only observations [11, 12, 13].

1.2 Fundamental Models

1.2.1 Precipitation particles and their electromagnetic properties

To numerically characterize integral properties of precipitation (such as the precipitation rate) within a radar observing volume, a good understanding of the distributions of properties such as the size and mass of precipitation particles is necessary. Paramount to this is the concept of Particle Size Distribution (PSD). Mathematically, the PSD is a function $N(D)$ that describes the density of precipitation particles of a given size within an elementary atmospheric volume. More precisely, $N(D)dD$ is defined as the concentration of precipitation particles with sizes between D and $D + dD$ in a specified volume of air. Given expressions that relate the size of a precipitation particle to its mass and electromagnetic backscattering properties, the PSD function may be used to derive relationships between the Liquid Water Content (LWC) and radar reflectivity. In a seminal study, Marshall and Palmer [15] showed that rain Drop Size Distributions (DSDs) follow an exponential distribu-

tion, i.e. $N(D) = N_0 \exp(-\lambda D)$. Although subsequent studies showed that DSDs are generally better described by gamma functions, $N(D) = N_0 D^\mu \exp(-\lambda D)$, (see Ulbrich [17] for a review), the exponential DSD formulation of [15] represented a milestone in meteorology because it set the stage for analytical investigations of the relationships between precipitation properties and radar observations. While initially focused preponderantly on rain, as measurement techniques improved, PSD studies started addressing ice particles in the early seventies (e.g. [18, 19]). It was found that, similarly to raindrops, ice PSDs may be accurately described by gamma functions.

Equally important to the description of PSDs is the quantification of the amount of radar power backscattered by precipitation particles. To simplify the analysis, the radar measurements of returned power are converted into a related variable called the equivalent radar reflectivity factor, defined as [14]:

$$Z = \frac{\lambda^4}{\pi^5 |K_w|^2} \int_0^\infty N(D) \sigma_b(D) dD \qquad (1.1)$$

where λ is radar frequency, $|K_w|$ is the dielectric factor of water, and $\sigma_b(D)$ is the backscattering cross-section of a precipitation particle of diameter D. The backscattering cross-section is the equivalent area that would isotropically return an amount of power equal to that actually returned by the precipitation particle [20]. The equivalent reflectivity factor is defined to equal $\int_0^\infty N(D) D^6 dD$ (in mm^{6}m^{-3}) for spherical rain drops in the Rayleigh regime. That is, for spherical raindrop whose diameter D satisfy the inequality $\frac{\pi D}{\lambda} < 1$, the backscattering cross-section $\sigma_b(D)$ is proportional to D^6. For DSD characterized by raindrops in the Rayleigh regime, the radar reflectivity Z defined $\int_0^\infty N(D) D^6 dD$ is a very simple but meaningful variable that can be calculated analytically as a function of the DSD parameters and readily determined from the power measured by radar. Consequently, the radar reflectivity has been established as the most meaningful and convenient variable to interpret the radar return power. When the precipitation particles do not fall in the Rayleigh regime, the general formulation given in Eq. (1.1) is used to interpret observations. It should be noted that the conversion from power to reflectivity (or equivalent reflectivity) is computationally the same, irrespective of whether precipitation particles are in the Rayleigh regime or not. However, the interpretation of observed radar reflectivity needs to account for the possibility of the precipitation particles not being in the Rayleigh regime.

When raindrops are too large relative to the radar wavelength, the Mie solution of Maxwell's electromagnetic equations is generally used to calculate $\sigma_b(D)$ [21]. While the Mie solution assumes spherical scatterers, large raindrops are oblate. Although the assumption of spherical raindrops is acceptable in many situations, there are radar applications when the oblateness of raindrops needs to be considered. In such applications, the electromagnetic properties of raindrops can be calculated using a more complex numerical methodology called the T-Matrix approach [22]. The use of the Mie solution in weather applications dates back to at least 1961 [20].

The quantification of the backscattering cross-section of ice particles is significantly more challenging than that of raindrops. This is because ice-particles exhibit a large variety of complicated shapes that preclude the application of straightfor-

ward electromagnetic equation solvers such those used in the Mie and T-matrix approaches. Before the emergence of computationally more general solvers, it was customary to assume that ice particles are spherical mixtures of ice and air characterized by an equivalent dielectric constant [20]. However, this assumption does not work well for ice particles large compared to the radar wavelength [23, 24, 25]. To address the need for accurate backscattering calculations (and electromagnetic scattering properties in general), several research groups started developing databases of ice particles and associated scattering properties using the Discrete Dipole Approximation (DDA) approach [26] and made them available to the science community at large [24, 25]. The drawback of DDA approach is its computational cost. Specifically, the complexity of ice particle shapes precludes the use of efficient spectral solvers that make use of analytical formulae that reduce the original equations to significantly simpler equations solvable in the Fourier space [28]. As a consequence, intensive numerical calculations are necessary to quantify the electromagnetic properties of ice particles. To circumvent the intensive numerical calculates, Hogan et al. [27] developed an approach based on the Rayleigh-Gans approximation that provides computational efficient yet accurate estimates of the electromagnetic properties of ice particles at microwave frequency. When available, scattering calculations based on the DDA or other numerically intensive methods are preferable, but such calculations are not available at all frequencies, especially for new sub-millimeter wavelength radiometers that have been only recently developed or are being developed for future space missions. For such frequencies and very large ice particles relative to the instrument's wavelength, the Rayleigh-Gans approximation of Hogan et al. [27] that together with the Mie-based approach of [21] and absorption models (e.g. Rosenkranz [29]) provide the ingredients necessary to simulate space-borne radar and radiometer observations from atmospheric geophysical variables.

Although valuable insight can be derived from analytical formulations of the PSDs, the increased availability of PSD observations from field campaigns eventually resulted in a paradigm shift regarding the use of the PSD observations in precipitation estimation methodologies. Specifically, it was found that a concentration scaling parameter N_w can be derived from observations without any assumption regarding the PSD shape and used along with a geometric scaling parameter, i.e. the volume weighted D_m, to accurately characterize all relevant PSDs and the associated radar and radiometer properties [30]. The concentration scaling parameter, also known as the generalized PSD intercept [31], is defined as

$$N_w = \frac{4^4}{\pi \rho_w} \frac{PWC}{D_m^4} \tag{1.2}$$

where PWC is the equivalent precipitation (either ice or rain) water content and D_m is the volume (or mass) weighted diameter. One of the most consequential implications of the normalized intercept is the fact that it can explain and mitigate variability in the relationships between radar observations and associated precipitation variables such as equivalent water content and rate. That is, representations of the joint distributions of reflectivities simulated from observed PSDs and the associated precipitation water content exhibit significant variability that makes the estimates the precipitation water
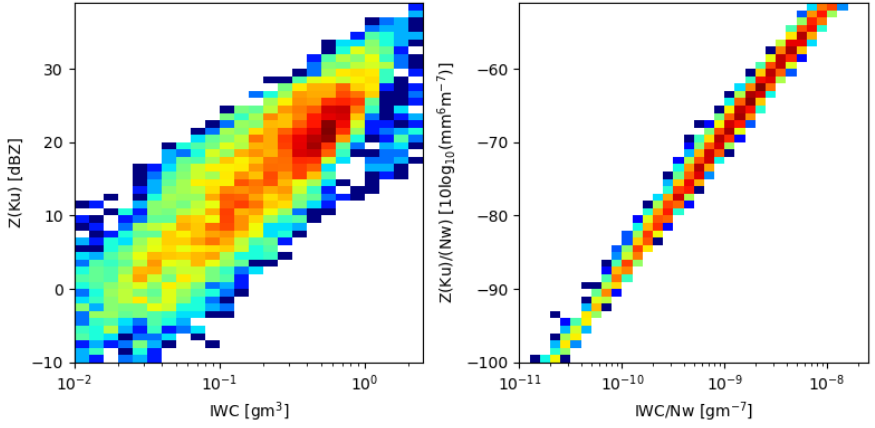
Figure 1.1   (Left) joint distribution of ice water content (IWC) and associated Ku-band reflectivity calculated from PSD observations from IMPACTS and (Right) joint distribution of normalized IWC and Ku-band reflectivity.

content from single frequency reflectivity observations highly uncertain. Shown in the left-hand panel of Fig. 1.2 is the joint distribution of IWC and associated reflectivity at Ku-band calculated using PSD observations from the NASA IMPACTS field experiment [33]. As apparent in the panel, the joint distribution is broad with a broad range of IWC values associated with any given reflectivity. However, normalization of both IWC and reflectivity by the associated N_w makes the resulting joint $(IWC/N_w, Z(Ku)/N_w)$ very narrow and close to a one-to-one function. This means that IWC/N_w can be accurately predicted from $Z(Ku)/N_w$. While normalization by itself does not eliminate uncertainties, because one needs information about N_w to derive a closed form solution for IWC, it does provide a general and physical consistent framework to investigate and mitigate uncertainties in space-borne radar and radiometer retrievals. This will be explained in detail in the next section. A remarkable fact regarding the normalization by N_w is that it collapses all radar-precipitation relationships (e.g. reflectivity vs precipitation rate, attenuation vs reflectivity, attenuation vs. precipitation rate etc.) to one-to-one functions for both ice and water [32].

1.2.2   Radar and radiometer models

The measured radar reflectivity at range r can be expressed as a function of the true radar reflectivity at range r, $Z(r)$, and the integrated attenuation along the path [34].

$$Z_m(r) = Z(r) \exp\left(-0.2\ln(10) \int_0^r k(Z(s))ds\right) \tag{1.3}$$

where $k(Z(s))$ is the specific attenuation at range s. The specific attenuation may be determined as a function of an observed or assumed analytical PSD using an equation similar to Eq. (1.1), i.e. $k = \int_0^\infty N(D)\sigma_e(D)dD$, with the extinction cross-section $\sigma_e(D)$ determined using one of the electromagnetic computational methodologies described in the previous section. When the specific attenuation and the reflectivity are related through a power law, i.e. $k = \alpha Z^\beta$ with β constant with range, a closed form solution for Z exists [34], i.e.

$$Z(r) = Z_m(r)/(1 - q \int_0^r Z_m^\beta(s)ds)^{1/\beta} \qquad (1.4)$$

where $q = 0.2\beta ln(10)$. This solution was first derived by Hitschfeld and Bordan [2] and started getting prominent in spaceborne radar applications with the work of [35], [36] and [34].

A particular challenge in applying Eq. (1.4) to radar observations affected by significant attenuation is that the numerical value of term $q \int_0^r Z_m^\beta(s)ds$ may become larger than 1.0, in which case the equation is not applicable anymore. Moreover, even if $q \int_0^r Z_m^\beta(s)ds < 1$ the path integrated attenuation associated with Eq. (1.4) may not be in agreement with estimates from a Surface Reference Technique (SRT) analysis. This is discussed in [36] and [34]. Several ad-hoc techniques were developed to reconcile solution 1.4 with the SRT estimates, but, fundamentally, the problem was not satisfactorily addressed from the physical perspective until the work of Ferreira et al. [32]. Ferreira et al. [32] noted that all $k - Z$, $Z - R$ or $Z - PWC$ (where k is the specific attenuation and Z, R and PWC are the associated reflectivity, precipitation rate and precipitation water content) are exact for a given constant N_w. They also noted that more general relationships, explicitly accounting for the N_w variability, need to be derived and used to make the Hitschfeld-Bordan solution in Eq. (1.4) consistent with SRT estimates of Path Integrated Attenuation (PIA). Specifically, a more general $k - Z$ relationship of the type

$$k = dN_w^{1-\beta} \alpha Z^\beta \qquad (1.5)$$

where dN_w is the ratio of actual N_w to that of the reference N_w^0 for which the relation $k = \alpha Z^\beta$ holds perfectly may be derived and used with 1.4. The PIA attenuation associated with the generalized $k - Z$ relation in 1.5 is

$$PIA_{HB}(dN_w) = -10/\beta \log_{10}(1 - qdN_w^{1-\beta} \int_0^{r_s} \alpha Z_m^\beta(s)ds) \qquad (1.6)$$

Given an independent estimate of PIA from the SRT, PIA_{SRT}, one may determine the value of dN_w that satisfy $PIA_{HB}(dN_w) = PIA_{SRT}$. This provides a physical approach to reconcile the Hitschfeld-Bordan solution with a potentially different SRT PIA estimate [32]. The benefit of this approach relative to more ad-hoc approaches such as the α adjustment method [34] is that it enables the adjustment of the $Z - R$ (or $Z - PWC$) used in the estimation of precipitation rates (or equivalent water contents) from the attenuation corrected reflectivities [32]. This is because systematically different mean particle sizes may result not only in biased attenuation correction, but also in biased precipitation estimates due to the application of a biased reflectivity

precipitation relationship. Therefore, the benefit of using N_w-based relationships is twofold [32].

It should be noted that because neither the SRT estimates nor the Hitschfeld-Bordan predictions of PIA are perfect, equating them exactly is suboptimal because it attributes various types of uncertainties to variability in the N_w. A better approach is to adjust N_w such that the final PIA_{HB} is consistent with both the uncertainties in its initial values (prior to the SRT based adjustment) and the PIA_{SRT} uncertainties. Iguchi et al. [37] developed such a methodology based on Bayes estimation theory. However, Iguchi et al. [37] did not update the Hitschfeld-Bordan solution in terms of N_w, but in terms of an equivalent variable ε, and it was Ferreira et al. [32] who made the connection between SRT estimates and N_w adjustments.

The use of normalized $k - Z$ and Z-precipitation relation is beneficial even when SRT PIA estimates are not available but additional sources of information, such as coincident radiometer observations are available. Specifically, if a set of observations Y_obs independent of the radar observations used in a radar-only precipitation profiling algorithm, one may tune the N_w assumptions made in the radar-only profiling algorithm to maximize the agreement between them and their prediction from the radar-only estimates. Or, more precisely, an objective function may be defined as

$$F(\mathbf{N_w}) = \frac{1}{2}(\mathbf{Y_{obs}} - \mathbf{Y}(\mathbf{Z_m}(\mathbf{N_w})))^{\mathbf{T}}\mathbf{W_Y^{-1}}(\mathbf{Y_{obs}} - \mathbf{Y}(\mathbf{Z_m}(\mathbf{N_w}))) +$$
$$\frac{1}{2}(\mathbf{N_w} - \mathbf{N_w^0})^{\mathbf{T}}\mathbf{W_N^{-1}}(\mathbf{N_w} - \mathbf{N_w^0}) \quad (1.7)$$

where $\mathbf{Y}(\mathbf{Z_m}(\mathbf{N_w}))$ is a numerical model that predicts observations $\mathbf{Y_{obs}}$ as a function of the space-borne radar observations $\mathbf{Z_m}$ and the normalized $\mathbf{N_w}$ intercepts. Matrix $\mathbf{W_Y^{-1}}$ quantifies uncertainties in model $\mathbf{Y}$, while $\mathbf{N_w^0}$ and $\mathbf{W_N}$ are the climatological values of $\mathbf{N_w}$ and their associated covariance matrix. Note that $\mathbf{Y_{obs}}$ may consist of any useful combination of space- or ground-based observations, while the set of N_w may need to be extended to include other geophysical variables relevant in the prediction of $\mathbf{Y}$. From the mathematical perspective, the problem of determining $\mathbf{N_w}$ from $\mathbf{Y_{obs}}$ is generally ill-posed and additional climatological, or "a priori" in statistical terminology, information is needed to derive a unique solution [38]. The additional information is provided by the second term of the objective function in Eq. (1.7). An implementation of a combined radar-radiometer estimation algorithm based on Eq. (1.7) and applicable to airborne observations was developed by Grecu and Anagnostou [39]. An evaluation based on synthetic observations derived from cloud resolving model simulations indicated the superiority of the relative to radar-only retrievals. A potentially more general approach, i.e. considering a larger set of state variables, but computationally more intensive and prone to challenges when used in operational environment had been developed by Marzano et al. [40]. Specifically, the state variables in [40] included the precipitation water contents while the radar observations were not implicitly satisfied but included in the optimization problem. A comprehensive discussion on why an approach with a reduced number of variables and the radar observations at a given frequency automatically satisfied in provided in [39].

Irrespective of whether single-frequency radar observations are included in the objective function or automatically satisfied, it should be noted that the use of additional information enables in theory the derivation of more accurate estimates of additional variables, such as the normalized PSD intercepts, that in the worst case scenarios are simply set up based on their climatology. To estimate the state variables in Eq. (1.7), a computationally efficient model to simulation the observations **Y** and an optimization procedure are needed. The simulation of air- and space-borne radiometer requires a procedure to solve the radiative transfer equation, which in the plane-parallel approximation reads [41].

$$\mu k_{ext}\frac{dI(\mu,\phi)}{dz} = -I(\mu,\phi)+(1-a)B(T)+$$

$$\frac{a}{4\pi}\int_0^{2\pi}\int_{-1}^1 p(\mu,\phi,\mu',\phi')I(\mu',\phi')d\mu'd\phi' \quad (1.8)$$

where $I(\mu,\phi)$ is the intensity in direction given by μ (the cosine of the angle between the actual direction and the vertical axis) and azimuthal angle ϕ, k_{ext} is the extinction coefficient, a is the scattering albedo (the ratio of the scattering coefficion to the extinction coefficients), $B(T)$ is the black body radiation emitted by the atmosphere at temperature T and the radiometer's frequency and $p(\mu,\phi,\mu',\phi')$ is the scattering function. The most general solvers of the radiative transfer equation are computationally intensive. However, the assumption of no azimuthal dependence and the approximation of I and $p(\mu,\mu')$ using the first two terms of a Legendre series [41] reduce the initial equation to a system of two coupled ordinary differential equations [41]. Systematic evaluations between the approximate solution and more general solutions revealed differences that can mitigate through simple modifications that account for geometric effects in the approximate solution [42].

The relevant coefficients in Eq. (1.8) are determined through the integration of the absorption, scattering and phase function properties of individual particles for given observed or analytical PSDs. A file containing the integrated scattering properties used in the GPM combined algorithm [43] is available in netCDF format at: https://github.com/mgrecu35/IET_bookChapter/tree/main/lookupTables. The properties of four types of hydrometeors, i.e. rain, snow, graupel and hail, are included in the file. Properties are calculated assuming normalized gamma particle size distributions with μ=2 and N_w=0.08cm^{-4}. The mean mass diameter, precipitation rate, and precipitation water content associated with each entry are also included in the file. The rain, graupel and hail properties are calculated using the Mie approach, while the snow properties are derived from DDA calculations. Additional information is provided in the README.md in the lookup table directory. An implementation of plane-parallel radiative solver of the [41] is available in directory src of https://github.com/mgrecu35/IET_bookChapter/. The reader is encouraged to pull the entire directory and examine the files in subdirectory examples. These files provide examples of radar and radiometer calculations using the concepts described in the chapter. The examples require an working version of Python and some specific library. Instructions on how the installation of the required library are provided in the README file in the examples directory.

1.2.3 Elements of optimal estimation theory

According to Gelb [44], an optimal estimator is a computational algorithm that processes measurements to deduce a minimum error (in accordance with some stated criterion of optimality). Based on this classical definition, any estimate that results from the minimization of an error-related objective function like the that in Eq. (1.7) is optimal. Nevertheless, because the minimization of observations errors is usually insufficient in deriving accurate estimates, additional terms called regularization terms [45] need to be included in the objective functions. An effective and meaningful type of regularization may be achieved through the use of Bayes' Theorem [46]. Bayesian optimal estimation is preferable to other types of regularizations when the variables to be estimated have well-defined physical models and their statistical properties may be systematically studied independently of the estimation problem at hand. This is the case for combined radar radiometer retrievals because the distributions of PSD intercepts can be independently studied and characterized using ground observations and/or numerical models.

Another element specific of optimal estimation procedure is their reliance on an optimization procedure. This is the reason why optimal estimation procedures are not always the method of choice in applications. Specifically, in some applications, the optimization problem associated with the estimation problem is so complicated that alternative (theoretically inferior) approaches are preferred.

The ensemble smoothing algorithm may be summarized as follows:

- Generate an ensemble of PSD intercepts N_w.
- Derive radar-only precipitation estimation from the Ku-band radar observations.
- Simulate radiometer, additional frequency radar (if multiple radar observations are available) and SRT PIA observations.
- Apply an Ensemble Kalman Smoother

$$\mathbf{X} = \mathbf{X} + \mathbf{cov}\langle\mathbf{X},\mathbf{Y}\rangle(\mathbf{cov}\langle\mathbf{Y},\mathbf{Y}\rangle + \mathbf{R})^{-1}(\mathbf{Y_{obs}} - \mathbf{Y(X)}) \tag{1.9}$$

to update the solution.

1.2.4 Additional matters

1.2.4.1 Non-uniform beam filling

1.2.4.2 Multiple-scattering

1.2.4.3 Radiance preprocessing

1.3 Example of GPM combined observations and retrievals

Shown in figure 1.3 is an example of DPR observed reflectivity and two of the associated brightness for a portion of orbit 5866 over the Kwajelein atoll. As apparent in the figure, at reflectivity observations tend to be significantly attenuated at Ka-band. Some scans exhibit attenuation even at Ku-band. As discussed in the previous sections, the reflectivity observations need to be corrected for attenuation to be usable in the derivation of precipitation estimates. Independent estimates of the PIA from the application of SRT method are extremely important in the attenuation correction
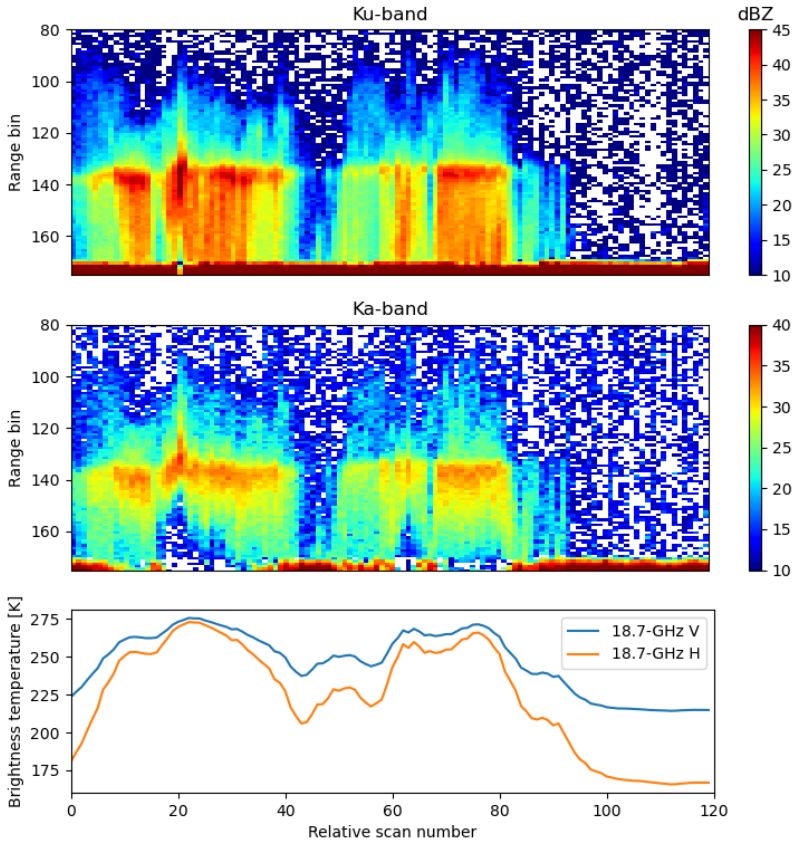
Figure 1.2 *Example of observed DPR Ku-(top), Ka-band reflectivities (middle), and GMI 18.7-GHz brightness temperatures (bottom).*

process. However, reliable SRT PIA estimates are not always available, especially when only single frequency radar-observations are available and the attenuation is low relative to the noise in the estimates. An assessment of the accuracy of the DPR PIA estimates from the single and dual frequency SRT method is provided in [47]. The 18.7-GHz brightness temperatures for orbit 5866 over the Kwajelein atoll are also shown in the bottom panel of Fig. 1.3. As explained in the previous section brightness temperatures at X-band and higher frequencies may be used to estimate provide alternative PIA estimates. Such estimates are especially useful when the SRT PIA are unreliable and may be used in the estimation process along with SRT PIAs, because the optimal estimation theory can effectively incorporate information from multiple sources as long as their uncertainties are properly specified.

1.4 Summary and conclusions

References

[1] Weinman JA, Meneghini R, Nakamura K. Retrieval of precipitation profiles from airborne radar and passive radiometer measurements: Comparison with dual-frequency radar measurements. Journal of Applied Meteorology. 1990; 200(29): 981 – 993.

[2] Hitschfeld W, Bordan J. Errors inherent in the radar measurement of rainfall at attenuating wavelengths. Journal of Atmospheric Sciences. 1990; 11(1): 58–67.

[3] Meneghini R, Eckerman J, Atlas D. Dermination of Rain Rate from a Space-borne Radar Using Measurements of Total Attenuation. IEEE Transactions on Geoscience and Remote Sensing.1983;GE-21;34–43.

[4] Fujita M, Okamoto K, Yoshikado S, Nakamura K. Inference of rain rate profile and path-integrated rain rate by an airborne microwave rain scatterometer. Radio Science. 1985; 20(3); 631–642.

[5] Smith E. Estimating 13.8-GHz pathintegrated attenuation from 10.7-GHz brightness temperatures for the TRMM combined PRTMI precipitation algorithm. Journal of Applied Meteorology. 1997; 36; 365–388.

[6] Kummerow CK. The Tropical Rainfall Measuring Mission (TRMM) sensor package. Journal of Atmospheric and Oceanic Technology. 1998; 15; 809–817.

[7] Haddad Z. The TRMM day-1 radar/radiometer combined rain-profiling algorithm. Journal of the Meteorological Society of Japan. 1997; 75; 799–809.

[8] Grecu M, Olson WS, Anagnostou E. Retrieval of precipitation profiles from multiresolution, multifrequency active and passive microwave observations. Journal of Applied Meteorology. 2004; 43; 562–575.

[9] Masunaga H. Combined radar and radiometer analysis of precipitation profiles for a parametric retrieval algorithm. Journal of Atmospheric and Oceanic Technology. 2005; 22; 909–929.

[10] Munchak J. A modular optimal estimation method for combined radar-radiometer precipitation profiling. Journal of Applied Meteorology and Climatology. 2001; 50; 433–448.

[11] Grecu M, Olson W.S. Bayesian estimation of precipitation from satellite passive microwave observations using combined radar retrievals. Journal of Applied Meteorology and Climatology. 2006; 45; 416–433.

[12] Kummerow C. An observationally generated a priori database for microwave rainfall retrievals. Journal of Atmospheric and Oceanic Technology. 2011; 28; 113–130.

[13] Hou A. The global precipitation measurement mission. Bulletin of the American Meteorological Society. 2014; 95; 701–722.

[14] Meneghini R, Kozu T. Spaceborne weather radar. Boston: Artech House Publ. 1990; ISBN: 0890063826.

[15]   Marshall JS, Palmer WMK. The distribution of raindrops with size. J. Meteorol. 1948, 5, 165–166.

[16]   J. S. Marshall and R. C. Langille and W. Mc K. Palmer", Measurement of rainfall by radar. Journal of Atmospheric Sciences. 1997; 4(6); 186–192.

[17]   Ulbrich CW. Natural variations in the analytical form of the raindrop size distribution. Journal of climate and applied meteorology. 1983; 22(10). 1764–1775.

[18]   Sekhon RS, Srivastava RC. Snow Size Spectra and Radar Reflectivity. Journal of Atmospheric Sciences. 1970; 27(2); 299–307.

[19]   Heymsfield A. Precipitation Development in Stratiform Ice Clouds: A Microphysical and Dynamical Study Journal of Atmospheric Sciences. 1977; 34(2); 367–381.

[20]   Battan LJ. Radar observation of the atmosphere. 1973.

[21]   Bohren CF, Huffman DR. Absorption and scattering of light by small particles. John Wiley and Sons. 2008.

[22]   Mishchenko MI, Travis LD, Lacis AA. Scattering, absorption, and emission of light by small particles. Cambridge university press; 2002 Jun 6.

[23]   Tyynelä J, Leinonen J, Moisseev D, Nousiainen T. Radar backscattering from snowflakes: Comparison of fractal, aggregate, and soft spheroid models. Journal of Atmospheric and Oceanic Technology. 2011 Nov;28(11):1365-72.

[24]   Liu G. Approximation of single scattering properties of ice and snow particles for high microwave frequencies. Journal of the atmospheric sciences. 2004 Oct 1;61(20):2441-56.

[25]   Kuo KS, Olson WS, Johnson BT, Grecu M, Tian L, Clune TL, van Aartsen BH, Heymsfield AJ, Liao L, Meneghini R. The Microwave Radiative Properties of Falling Snow Derived from Nonspherical Ice Particle Models. Part I: An Extensive Database of Simulated Pristine Crystals and Aggregate Particles, and Their Scattering Properties Journal of Applied Meteorology and Climatology. 2016 Mar 1;55(3):691-708.

[26]   Draine BT, Flatau PJ. Discrete-dipole approximation for scattering calculations. Josa a. 1994 Apr 1;11(4):1491-9.

[27]   Hogan RJ, Honeyager R, Tyynelä J, Kneifel S. Calculating the millimetre-wave scattering phase function of snowflakes using the self-similar Rayleigh–Gans Approximation. Quarterly Journal of the Royal Meteorological Society. 2017 Jan;143(703):834-44.

[28]   Trefethen LN. Spectral methods in MATLAB. Society for industrial and applied mathematics; 2000 Jan 1.

[29]   Rosenkranz, P.W. Water vapor microwave continuum absorption: A comparison of measurements and models. Radio Sci. 1998, 33, 919–928.

[30]   Testud J, Oury, S, Black RA, Amayenc P, Dou X. The Concept of "Normalized" Distribution to Describe Raindrop Spectra: A Tool for Cloud Physics and Cloud Remote Sensing. Journal of Applied Meteorology, (2001). 40(6); 1118–1140.

[31]   Bringi VN, Chandrasekar V, Hubbert J, Gorgucci E, Randeu WL, Schoenhuber M. Raindrop size distribution in different climatic regimes from disdrom-

eter and dual-polarized radar analysis. Journal of the atmospheric sciences. 2003 Jan;60(2):354-65.

[32] Ferreira F, Amayenc P, Oury S, Testud J. Study and tests of improved rain estimates from the TRMM precipitation radar. Journal of Applied Meteorology. 2001 Nov;40(11):1878-99.

[33] McMurdie LA, Heymsfield GM, Yorks JE, Braun SA, Skofronick-Jackson G, Rauber RM, Yuter S, Colle B, McFarquhar GM, Poellot M, Novak DR. Chasing Snowstorms: The Investigation of Microphysics and Precipitation for Atlantic Coast-Threatening Snowstorms (IMPACTS) Campaign. Bulletin of the American Meteorological Society. 2022 May;103(5):E1248-74.

[34] Iguchi T, Meneghini R. Intercomparison of single-frequency methods for retrieving a vertical rain profile from airborne or spaceborne radar data. Journal of Atmospheric and Oceanic Technology. 1994 Dec;11(6):1507-16.

[35] Meneghini R, Eckerman J, Atlas D. Determination of Rain Rate from a Spaceborne Radar Using Measurements of Total Attenuation. IEEE Transactions on Geoscience and Remote Sensing, vol. GE-21, no. 1, pp. 34-43, Jan. 1983, doi: 10.1109/TGRS.1983.350528.

[36] Marzoug M, Amayenc P. Improved range-profiling algorithm of rainfall rate from a spaceborne radar with path-integrated attenuation constraint IEEE Transactions on Geoscience and Remote Sensing, vol. 29, no. 4, pp. 584-592, July 1991, doi: 10.1109/36.135820.

[37] Iguchi T, Kozu T, Meneghini R, Awaka J, Okamoto KI. Rain-profiling algorithm for the TRMM precipitation radar. Journal of applied meteorology. 2000 Dec;39(12):2038-52.

[38] Tarantola A. Inverse problem theory and methods for model parameter estimation. Society for industrial and applied mathematics; 2005 Jan 1.

[39] Grecu M, Anagnostou EN. Use of Passive Microwave Observations in a Radar Rainfall-Profiling Algorithm Journal of Applied Meteorology, 41(7), 702-715.

[40] Marzano FS, Mugnai A, Panegrossi G, Pierdicca N, Smith EA, Turk J. Bayesian estimation of precipitating cloud parameters from combined measurements of spaceborne microwave radiometer and radar. IEEE Transactions on Geoscience and Remote Sensing. 1999 Jan;37(1):596-613.

[41] Kummerow C. On the accuracy of the Eddington approximation for radiative transfer in the microwave frequencies. Journal of Geophysical Research: Atmospheres. 1993 Feb 20;98(D2):2757-65.

[42] Liu Q, Simmer C, Ruprecht E. Three-dimensional radiative transfer effects of clouds in the microwave spectral range. Journal of Geophysical Research: Atmospheres. 1996 Feb 20;101(D2):4289-98.

[43] Grecu M, Olson WS, Munchak SJ, Ringerud S, Liao L, Haddad Z, Kelley BL, McLaughlin SF. The GPM combined algorithm. Journal of Atmospheric and Oceanic Technology. 2016 Oct 1;33(10):2225-45.

[44] Gelb, A. Applied Optimal Estimation. The M.I.T. Press.

[45] Doicu A, Trautmann T, Schreier F. Numerical regularization for atmospheric inverse problems Springer Science and Business Media; 2010 Jul 16.

[46]   Maahn M, Turner, DD, Löhnert U, Posselt DJ, Ebell K, Mace GG, Comstock JM. Optimal Estimation Retrievals and Their Uncertainties: What Every Atmospheric Scientist Should Know. Bulletin of the American Meteorological Society. 2020; 101(9), E1512-E1523.

[47]   Meneghini, R., Kim, H., Liao, L., Jones, J.A. and Kwiatkowski, J.M., 2015. An initial assessment of the surface reference technique applied to data from the dual-frequency precipitation radar (DPR) on the GPM satellite. Journal of Atmospheric and Oceanic Technology, 32(12), pp.2281-2296.